MSNW

16436 SE 39th Place
Bellevue, WA 98008
Phone: (425) 644-2321
EMAIL: MSNWemail@yahoo.com

Propagating Magnetic Wave Plasma Accelerator (PMWAC) for Deep Space Exploration

Phase-I Final Report

TABLE OF CONTENTS

Introduction

For man to explore the solar system, a radically different propulsion system must be envisioned to make deep space missions possible. The requirements for deep space exploration are two-fold. First, there must be a power source that employs a fuel with a very high specific energy. This fuel must also be available in sufficient quantity for long missions. It is recognized that nuclear fission[1] and fusion[2] are the only reasonable sources that can be readily employed in the near future. Nuclear fission has been well developed and is available now. Plasma based fusion may be the most attractive, but awaits a breakthrough technology that would make it suitable for propulsion. Second, there must be an efficient method for converting this energy into the thrust and I_{sp} necessary for a fast mission at high power. It is proposed here to solve not only the second problem, but to provide the breakthrough technology required to make fusion propulsion a realizable goal in the next decade. The essential element by which these major challenges are solved is the propagating magnetic wave accelerator (PMWAC). Like a particle accelerator, an electromagnetic interaction is used to convey momentum to the plasma, and terminal speeds approaching the speed of light are at least theoretically possible. . In order to achieve significant thrust, unlike a particle accelerator, the propagating field acts on a much more massive entity - a magnetically self-confined plasmoid through the $\mathbf{j_p x B_{acc}}$ force acting on the plasma currents. The ideal plasmoid for acceleration is that commonly referred to as a Field Reversed Configuration (FRC)[3]. The FRC equilibrium has the highest possible mass for a given confining field energy. The FRC is magnetically insulated from the accelerator wall by the accelerator field, but it is magnetically isolated from the accelerator magnetic field as well. There is thus no thermal contact between the propellant (FRC) and the accelerator, and no problem in detachment of the plasma from the thruster magnetic fields that plague other propulsion schemes based on magnetic containment.

The acceleration scheme proposed here will allow for orders of magnitude increases in Isp over conventional electric propulsion with efficiencies that approach unity. The physical requirements for the accelerator are quite modest. In the prototype accelerator constructed in Phase I, a terminal wave speed of $4x10^5$ m/s was achieved with a field acceleration of $4x10^9$g. The accelerator mass was~ 30 kg. Operated at a duty cycle of ~ 10%, the directed thrust power from the accelerator would be > 1 MW. A proof of principle experiment demonstrating repetitive FRC formation and acceleration at this power level is the goal of the next phase.

Advanced Concept Background

Mission Requirements

Despite the present emphasis on manned missions that will culminate in the assembly of a permanent space station in low Earth orbit, human missions to the planet Mars and beyond continue to captivate the imagination of both scientists and laymen alike. Such missions embody the ultimate expression of human adventure and exploration. Steady, albeit limited, efforts to map out human exploration scenarios have continued. All scenarios have in common the major requirement of an energy source suitable for such endeavors, and a means for converting that power into thrust at high exhaust velocity. One hard fact that man has learned from long-term exposure to space is that any planetary mission must be measured in months and not years. It is clear that propulsion based on chemical energy lacks the requisite exhaust velocity ($<10^4$ m/s) and specific energy. The remaining possibilities are space nuclear power[1] and solar power[4]. Only nuclear power has shown sufficient development of the magnitude of power necessary for manned space flight, which must be at the several megawatt level. The reason for this can be seen from the following simple analysis. The power P required to accelerate a spaceship mass of mass M_{ss} to characteristic velocity v_c. in a time τ can be expressed approximately as:

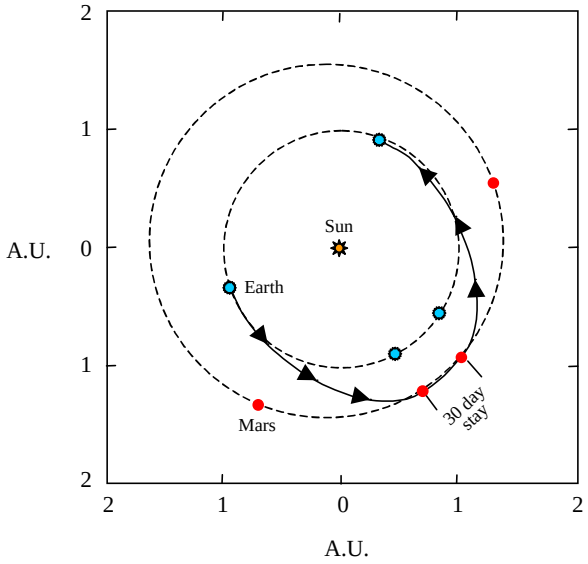

Figure 1. Fast mars mission showing 101 day inbound and 104 day outbound legs.

$$P \approx \frac{M_{ss} v_c^2}{2\tau} \qquad (1a)$$

from which one defines $v_c = (2\alpha\tau)^{1/2}$, where the specific power, $\alpha = P/M_{ss}$. Solving for the time to travel a distance S ($\sim v_c/2\cdot\tau$) yields

$$\tau(\text{months}) = 2\,\frac{[S(\text{astronomical units})]^{2/3}}{[\alpha(\text{kW/kg})]^{1/3}} \qquad (1b)$$

where a more "practical" length unit is used.

For an optimized rapid Mars transit[5] (see Fig. 1) $\tau \sim 3$ months, S ~ 2 AU, and one finds from eq. (1b) that $\alpha \sim 1$ kW/kg. For a spacecraft mass of 100 MT, one finds a power requirement of 100 megawatts. This power requirement is well beyond what can be provided by currently envisioned solar power sources (< 100 kW), and can only be met by nuclear fusion or fission. Fusion may still be years away from practicality, but will most likely be the energy source of choice once it is developed. Fission electric power is available now, and has been used safely in both submarines and aircraft carriers for years at the power levels envisioned here.

Regardless of foreseeable developments in this area, propulsion systems will be inherently power-limited. Thus, for example, the attainment of high exhaust-velocity or specific impulse (Isp) comes at the expense of vehicle thrust. This unfortunate situation can be alleviated

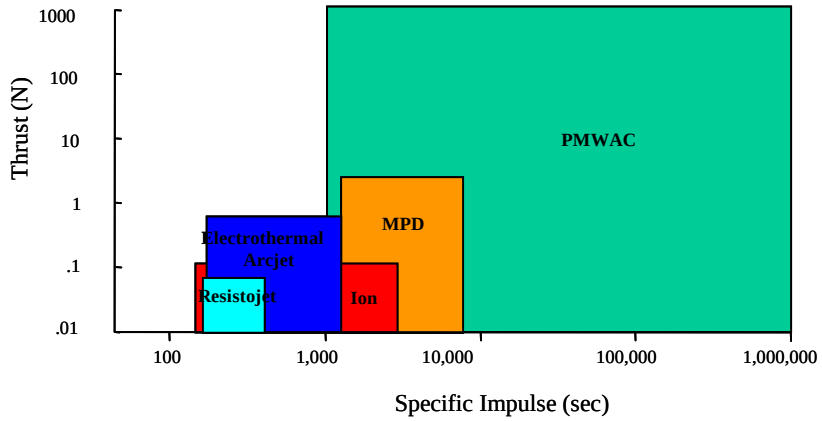

Fig. 2. Operational domains for various electric propulsion devices

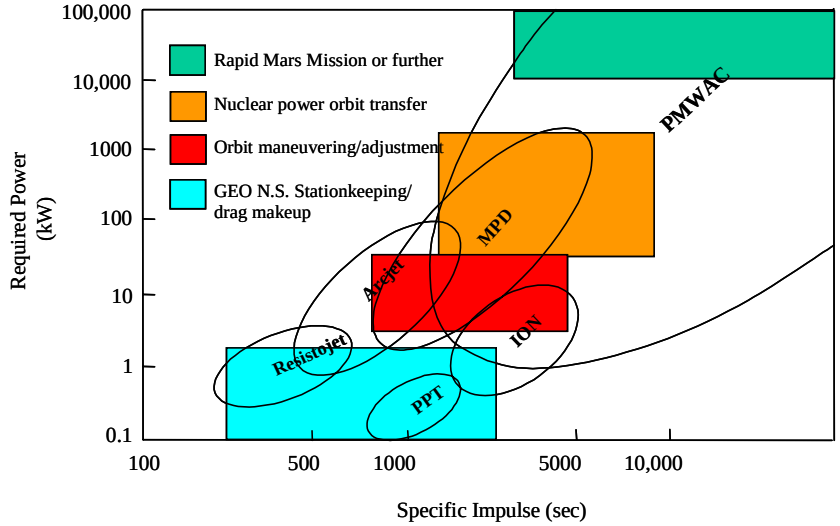

by the continuous modulation of the rocket exhaust, permitting considerably shorter transit times with reasonable payload. The ability to vary both thrust and Isp over a very wide range, and at a magnitude far beyond what could be envisioned with any other plasma thruster yet designed, is at the heart of the accelerator proposed here. The considerable improvement in performance and capabilities envisioned for PMWAC is illustrated in Fig. 2.

Technical Background

The plasmoid that will be accelerated in the PMWAC is formed and initially accelerated by the source coil set. The type of plasma that is generated by the source has its origin in the magnetic fusion program where it is commonly referred to as a Field Reversed Configuration (FRC). FRCs are compact toroidal plasmas confined usually in a cylindrical magnetic chamber, and without any significant toroidal magnetic field. A sketch of the geometry is shown in Fig. 3, and a somewhat dated review of the subject is given in Ref. 3. The FRC has such unique properties that it appears to have been designed solely with propulsion applications in mind. These properties are listed below.

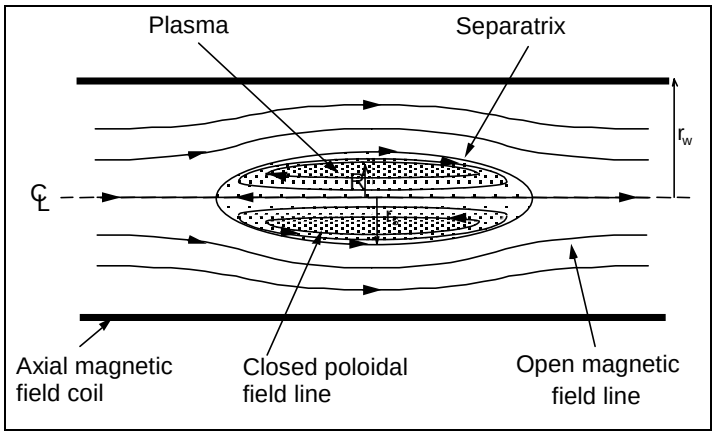

Figure 3. FRC Geometry Showing Flux Surfaces

1. Simple, linear, low field magnet system.

2. High plasma pressure. Radial pressure balance requires the plasma energy density, $nkT, \cong B^2/2\mu_0$, that of the axial magnetic field.

3. Easily translated and accelerated axially by changes in the external axial field.

4. Directed, unobstructed linear exhaust of detrapped plasma that can be ejected out either end with a simple magnetic mirror field.

The same attributes that make FRCs ideal for propulsion applications also make them the most attractive engineering option for terrestrial fusion power generation. Relative to the tokamak, the development of the concept has not been vigorously pursued. This has been due partly to the early historical success of the tokamak and partly for political reasons (rapid development of a scientifically proven confinement scheme).

For propulsion applications, it is desirable that most of the plasma be retained in the FRC as it is accelerated and expelled from the accelerator. The rate of FRC acceleration observed in experiments performed by the author at the University of Washington[6] was ~ 10^{10} m/s^2 which was by no means a maximum. Less than 100 μsec would thus be required to attain exit velocities of 10^6 m/s.

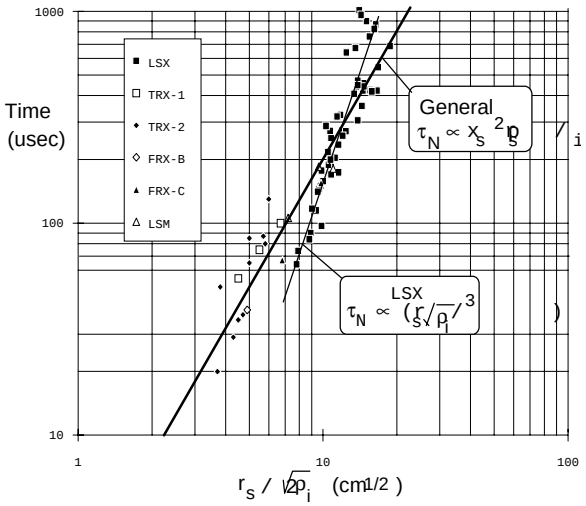

Figure 4. Measured FRC Particle Lifetime Scaling

Lifetime scaling results from FRC experiments[7] are shown on Fig. 4. The results from the largest FRC experiment, LSX, showed particle confinement of ~ 1 ms, with a strong radius r_s.and density scaling[8] (The ion gyroradius $\rho_i \sim n^{-3/5}$ for the FRC). Virtually all FRCs formed in LSX had lifetimes in excess of 100 μsec. Most of the data points were at 1-3x10^{21} m^{-3} densities, about an order of magnitude higher than for any other magnetic fusion device due to the inherently high β - the ratio of plasma energy to external confining magnetic field energy (<β> ~ 1 for the FRC). In the FRC acceleration experiments at the UW the plasma density was increased to over 10^{22} m^{-3}, with little particle loss observed during the acceleration process.

FRC Source

The FRC plasma to be accelerated to high velocity is generated in the source coil like that shown in Fig. 5, a prototype of which was built by MSNW and the University of Washington (UW) under a NASA Phase I STTR contract.

The formation sequence used to generate the FRC is shown below in Fig. 5. In the source the FRC is simultaneously formed and accelerated into the PMWAC coils at high velocity. There is a very wide range in both thrust and I_{sp} achievable with minor changes in formation fields, timing, and fuel. It should be noted that the rocket is completely shielded magnetically from the ejected plasma, and the ejected plasma is completely charge neutral so that there is no charge flow to the spacecraft. There is also vacuum insulation between the ejected plasma and spaceship so that there is no heat conducted from the rocket exhaust to the spacecraft. This magnetic insulation is maintained throughout the PMWAC.

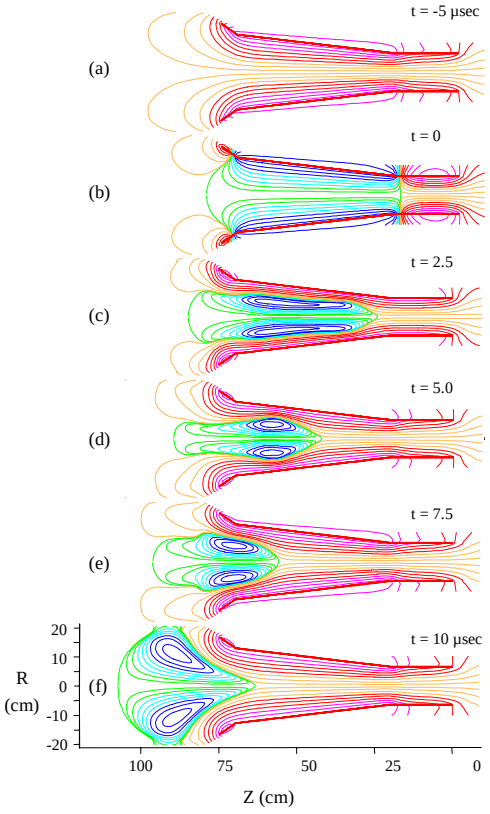

Figure 5. Results of 2D MHD calculations for inductive FRC formation in the source coil. Plotted are flux contours where the scale is reset for each time. FRC flux is denoted by green-cyan-blue lines. FRC mass was 0.06 mg Deuterium (20 mTorr D_2).

Most laboratory FRCs are neutrally stable to translational motion since the flux conserving coils are of constant radius and flux. If there is any difference axially in field across the FRC, the FRC is accelerated in the direction of lower field. During formation in the source coil shown

in Fig. 5, this axial field gradient will always be present due to the radial taper in the main (source) flux coil. Using a fully resistive two-dimensional magneto-hydrodynamic code (2D MHD) the entire formation process can be numerically calculated. This code has been used for many years on several experiments, and reproduces the experimentally observed FRC behavior with a high degree of accuracy[9]. The flux plots shown in Fig. 5 are the results of such calculations for the source coil. The initial steady field (<B> = 0.1 T) is shown in Fig. 5a. In the remaining sequence, the field is reversed only in the source coil section (b): During the initial reversal, weakly ionized plasma is formed due to the induced electric field, E_θ. The field is subsequently reversed but due to the presence of the low-density plasma, a strong diamagnetic current now flows, trapping the plasma in its own self-generated field. (c): With the continued flux increase in the source coil, the plasma becomes increasingly isolated from the coil boundary and heated by both compression and Ohmic dissipation. When the field external to the FRC, B_e, reaches a maximum ~ 0.3 T in (d), the plasma density, n is ~ $1x10^{21}$ m^{-3}, and the electron and ion temperatures, T_e, T_i ~ 20 eV.

Large voltages and magnetic fields have been employed in the past in order to obtain fusion relevant conditions during the formation of the FRC. Ion temperatures kT_i > 1 keV have been readily produced in this manner. For propulsion however, high exhaust plasma temperatures are unnecessary and in fact an inefficient use of energy. In experiments at the UW on the NASA funded STX experiment, it was found that FRCs could be formed inductively at very low

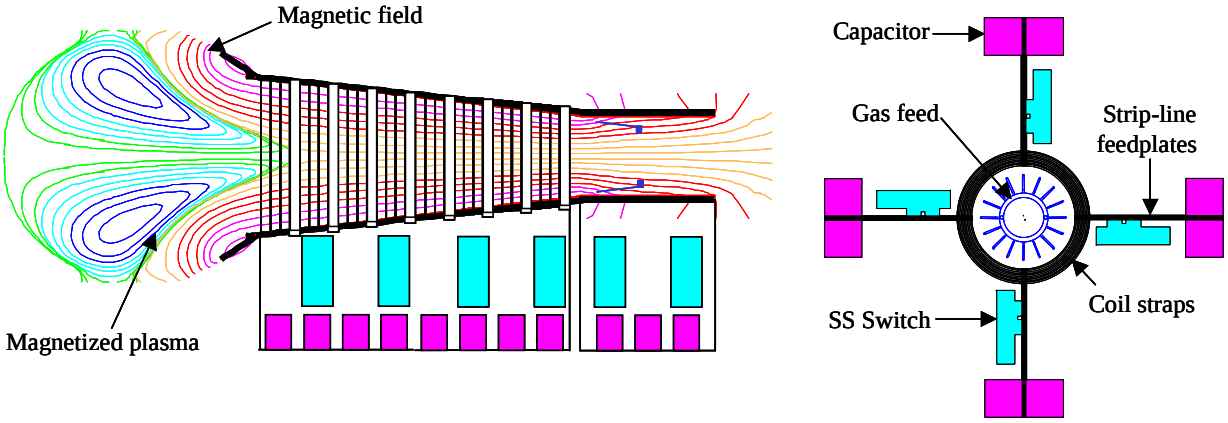

Figure 6. Schematic of the FRC source coil as built

voltages and fields[10]. In fact, low enough that the voltage and current required for field reversal was in the range of solid-state devices such as the Isolated Gate Bipolar Transistor (IGBT). This allows for the repetitive formation of FRC's with negligible switch losses.

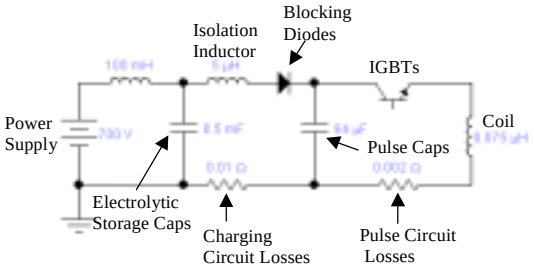

Figure 7. Schematic of pulse charging circuit as it was employed in Fig.8 for recharging the pulse caps for repetitive pulsing.

A repetitive source was developed at MSNW based on solid-state switching and the simple formation technique described in Fig. 5. A schematic of the device is shown in Fig. 6. The magnet was operated in a repetitive mode using a simple pulse charging circuit shown in Fig. 7. The resulting magnet current waveform is found in Fig. 8. The fields achieved were those employed in the calculation shown in Fig. 5. A plasma test was

conducted at the University of Washington by mounting the device over a conically shaped vacuum chamber at the end of the STX device. FRCs were formed and ejected into the STX main chamber. There was neither the time or funding to fully explore operation of this source, but a reasonable estimate of the thrust efficiency could be made from the measurements taken when the source was operated in single pulse mode.

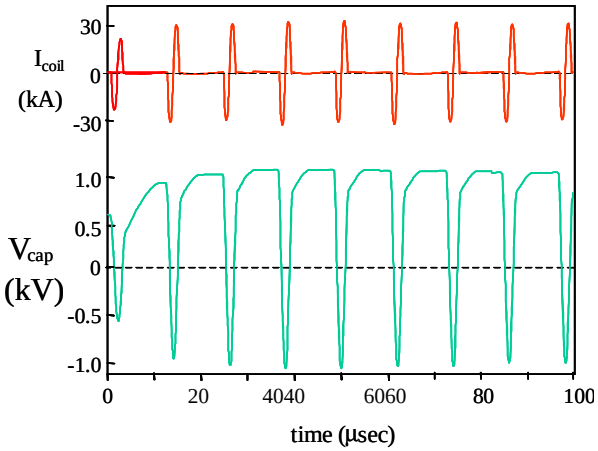

Fig. 8 Experimental waveforms from source coil in repetitive mode using the charging circuit shown in Fig 7.

A preliminary energy inventory for the source can be found in the table below. The overall efficiency, will improve dramatically as the Isp is increased with PMWAC, since the ionization 'tax' will become a smaller fraction of the total energy transferred to the plasma. As will be discussed in more detail, the electrical efficiency of the accelerator by itself is quite high. As indicated in the table below, if it were employed to accelerate the FRC plasmas ejected from the source coil as tested on STX, the resultant efficiency would rise from ~ 50% to 90%. With roughly 100 J of directed energy leaving with the FRC per pulse, and at a rep rate of 10 kHz (half the rep rate tested in these experiments), the net thrust power would be 1 MW.

TABLE I

ENERGY PARAMETER (J)	Value	PARAMETER	Value
Initial (Final) Stored Energy	75 (49)	Radiation losses	0.03
Total Energy lost from circuit	26	Energy left in FRC after ejection	3
Ionization losses	10	Thrust Energy (1/2 M v^2)	14
Source Efficiency (%)	**50**	Isp (s)	5,300
PMWAC supply cap stored energy	100 (10)	Final Thrust Energy	104
Energy transfer during acceleration	90	Final Isp	14,400
Final Overall Thruster Efficiency (Source + PMWAC) $\rightarrow$ 90%			
Final Jet Power to Total Thruster Mass (@10 kHz) = (900 + 140) kW/(22 kg + 40 kg) = 17 kW/kg			

Experimental background and motivation for PMWAC

As pointed out by Chang-Diaz et al.[5], a propulsion system that is capable of high and variable I_{sp} at high power is essential for a fast Mars mission. The necessary I_{sp} profile for this mission is found in Fig. 9. The source coil alone can not the higher values of I_{sp} required. The use of the PMWAC however can increase the I_{sp} to well beyond the range necessary for this mission, and would enable missions to the outer planets as well.

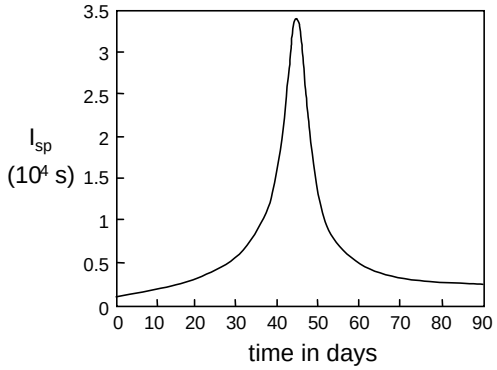

Figure 9. I_{sp} profile for rapid transit to Mars. I_{sp} and thrust are exchanged at constant power (10 MW).

To efficiently accelerate FRCs to high velocities another acceleration method other than the simple tapered coil used in the source coil must be employed. The reason for this is that a pulsed tapered coil has a continuously dropping field as the radius increases ($B_e \sim 1/r^2$) due to the flux conservation along the length of the coil. The force on the FRC therefore decreases rapidly as the FRC moves down the coil. However, the field (and thus pressure) gradient can be maintained across the FRC by the axial sequencing of a series of constant, or even better, decreasing radius coils in a manner that keeps the magnetic field high on the upstream side and low on the downstream side. The FRC then "surfs" on a magnetic pulse that moves axially along the accelerator (see Fig. 10). This was the technique employed in the UW TRAP experiments. In these experiments, the acceleration section was only 2 m long, yet velocities ~ 2.5×10^5 m/s were achieved.

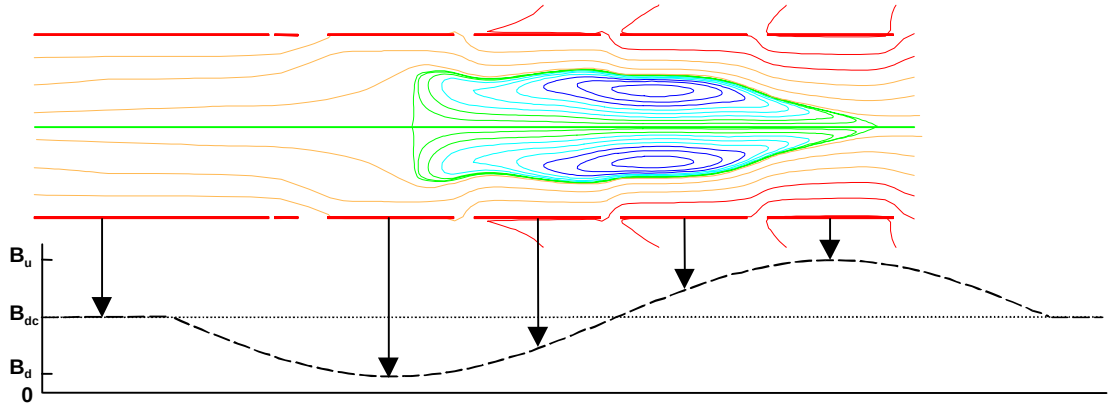

Figure 10. Upper plot of flux contours were taken from numerical calculations based on data from discharge 1647 during the acceleration of an FRC on the TRAP experiment. Bottom plot indicates the phasing of the accelerator coils, showing the point where each coil has reached at the time of the calculation..

By matching the timing and risetime of the coils, one can create, in the frame of the FRC, a quasi-steady field configuration shown in Fig. 10. Under these conditions the acceleration of the FRC is a constant. To first order, for the conditions above, the accelerating axial force is given simply by:

$$F_z = \frac{4}{\mu_0} \Delta B_z \ \varphi_i \qquad (2)$$

where φ_i is the FRC internal poloidal flux, and ΔB_z is the difference between the magnetic field outside the FRC on the upstream side, and the downstream field. For the STX source experiments, the Deuterium FRC formed had a mass of 10 μg, and a closed internal flux of φ_i ~ 0.4 mWb. The PMWAC device that was built and tested in Phase I had a length of 1.8 m. If one desires the final parameters given in the table above, the work done on the FRC should be equal to the energy loss from the storage capacitor, which is ~ 90 J. This implies a constant force of 50 N in the accelerator. From eq. 2, to achieve the necessary force, the upstream magnetic field must exceed the downstream field by ~ 0.04 T (or 400 G). Even for a downstream field of 0.02 T, the maximum magnetic pressure that the accelerator coils experience is ~ 0.2 psi. The accelerator coils can therefore be low mass. In the PMWAC device the thin (~ 0.4 mm) copper sheet employed was more than sufficient. Even for the higher energy applications to be discussed later, the magnetic forces are never a factor in the accelerator mass.

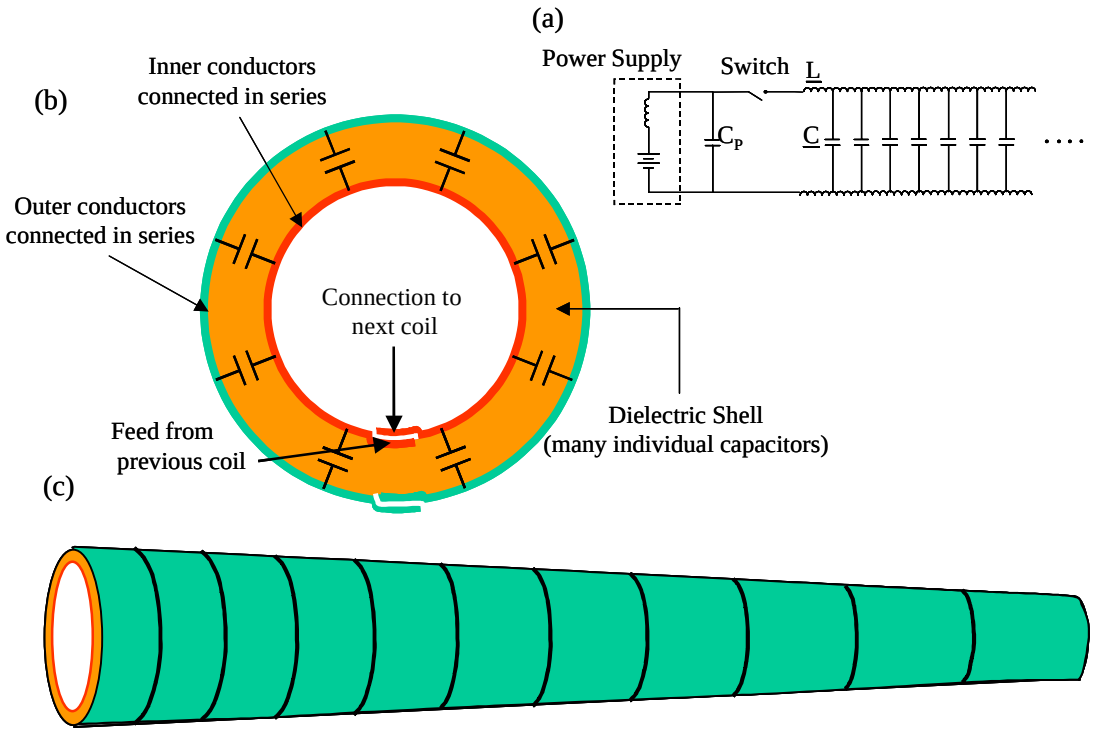

Figure 11. (a) Schematic electrical diagram of the propagating magnetic wave plasma accelerator (PMWAC). The inductance and capacitance are distributed continuously throughout the coil. (b) The dielectric material between the inner and outer helix provides the capacitance. (c) An indication of how the coil radius and turn length can be slowly varied to change the propagation speed along the coil length.

The large mass and inefficiency of the switching used in the large scale accelerator used in the TRAP experiments make a straight forward application of this method unsuitable for space applications. The accelerator inefficiency and the complex switching requirements can be eliminated by adopting a traveling wave line[11] for the acceleration in the manner shown in Fig. 11.

The use of such a line requires only one switch and one capacitor to generate a current (magnetic) pulse that propagates along the line. The propagation velocity v_p and accelerator impedance Z are given by the usual expressions for a transmission line:

$$v_p^2 = \frac{1}{LC} \qquad Z^2 = \frac{L}{C} \tag{3}$$

where L and C are the inductance and capacitance per unit length respectively. The double winding (outbound on the inner coil, and the return on the outer coil) assures that there is no net axial current flow in the line at any point. A net current would generate a non-symmetric force on the FRC. The capacitance is placed in the gap created between the conductors. The coil gap dimension δ can be stated in terms of the applied voltage V and the dielectric strength ε_S of the dielectric material if it is assumed that it is used at its maximum useful value, i.e. $\delta = V/\varepsilon_S$. The capacitance per unit length is then given by:

$$C = \frac{2\pi R_c \varepsilon_0 \kappa \varepsilon_S}{V}, \tag{4}$$

where κ is the relative dielectric constant of the material. The inductance per unit length is given by

$$L = \mu_0 \pi R_c^2 n^2 \tag{5}$$

where n is the number of turns per unit length. For a long solenoid the axial magnetic field is given by $B = \mu_0 nV/Z$. Using this expression along with eqs. (3) and (5), one can solve for R_c:

$$R_c = \frac{2V\kappa\varepsilon_S}{c^2 B^2}. \tag{6}$$

The propagation velocity can also be determined from eqs. (3), (4), and (5):

$$v_P = \left[\frac{2V}{R_c^3 \kappa \varepsilon_S}\right]^{1/2} \frac{c}{2\pi n}. \tag{7}$$

Both the magnetic force as well as the velocity of propagation is increased with increasing voltage so that PMWAC was built to operate with an initial charge voltage of 25 kV. This lies within the operating range of stacked solid-state switches[12]. A dielectric with a large $\kappa\varepsilon_S$ product allows for reasonable values of R_c. The ideal dielectric with by far the large $\kappa\varepsilon_S$ product is the ferro-electric, barium titanate (BaTiO), where $\varepsilon_S = 5\text{x}10^6$ V/m and $\kappa \sim 2500$. This was the capacitor dielectric that was employed in the PMWAC device. An additional advantage of BaTiO is the very low dissipation factor at high frequency and voltage. Employing this material and at the voltage given above, one finds that for a propagating magnetic field as high as 0.4 T, eq. (6) indicates that the coil radius be about 4.3 cm. The propagation velocity scaling from eq. (7) becomes

$$v_P = \frac{1.35\text{x}10^5}{R_c^{1.5} n}\ \text{m/s}. \tag{8}$$

For an initial coil radius R_c of 0.14 m and an n of 12 turns per meter (close to that of the PMWAC device built), the initial propagation velocity from eq. (8) is $2\text{x}10^5$ m/s ($1.8\text{x}10^5$ m/s

observed). An order of magnitude increase in velocity could readily be achieved by a modest decrease in radius or n. This is accomplished by a slow variation in these parameters along the length of the accelerator. In the prototype PMWAC device, the acceleration was achieved by varying only the radius.

PMWAC device construction and operation

The design point for the prototype PMWAC was chosen to test the concept with a magnetic wave velocity, acceleration, and magnitude greater than would be required for a high powered electric thruster alone. The reason for this was twofold: to confirm the suitability of the method for power-limited electric propulsion, but also test the feasibility of this accelerator approach in obtaining the conditions by which nuclear fusion could be achieved and employed as the propulsion power source in a simple, straightforward way.

The actual device differed from the conceptual picture presented in the previous section in the following ways. To simplify the construction, the coil was divided into 12 cylindrical sections each with a length of 0.15 m. Thus the current flowed azimuthally around each coil, and then axially across the small 2 cm gap between coils to the next coil. The coils were connected

Fig. 12. PMWAC device

in a manner so that the return currents in the outer coil flowed in the opposite direction in the gap to that in the inner coil, but in the same azimuthal direction in the coil itself. In this manner the field generated was purely axial. With the inner and outer coils carrying the same current, the accelerator had effectively twice the turns per unit length and thus twice the field magnitude. A schematic of a coil in cross-section is shown in Fig. 11b. A picture of the device is found in Fig. 12.

Ideally, one would have the dielectric material constructed in such a manner as to fill the entire gap between outer and inner coils. In addition the coils would be bonded directly onto these cylindrical capacitors. These steps would ensure the highest possible efficiency and lowest dissipation for the accelerator. Such an arrangement would be feasible given a much higher level of funding, but for the initial prototype, individual capacitors were used. In order to have the needed flexibility as well as provide a good approximation to a distributed capacitance, A large number (~ 4000) 1 nF, Class I, 20 kV BaTiO capacitors were soldered between the inner and outer coils of the

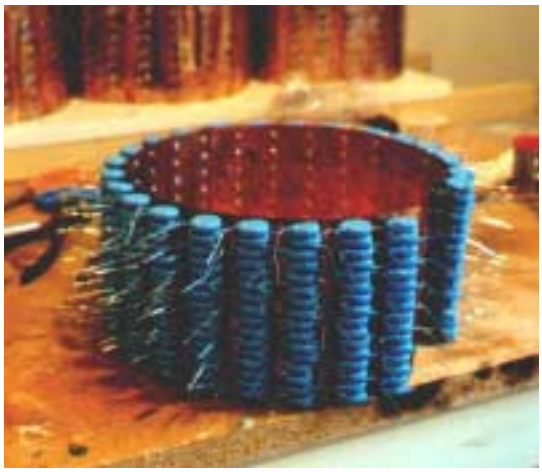

Figure 13. Assembly of PMWAC coil turn

accelerator. A picture of one of the coils during assembly is found in Fig. 13. Since it was desired to operate at high wave speeds (i.e. frequency), a very high quality capacitor was used. This, plus the less than unity filling fraction from the shape of the capacitors, reduced the maximum possible capacitance per unit length inferred by eq. (4) by roughly a factor of 2. Since there was more than enough voltage capability for the magnetic field desired (0.1 T), the increase in line impedance was found to be unimportant.

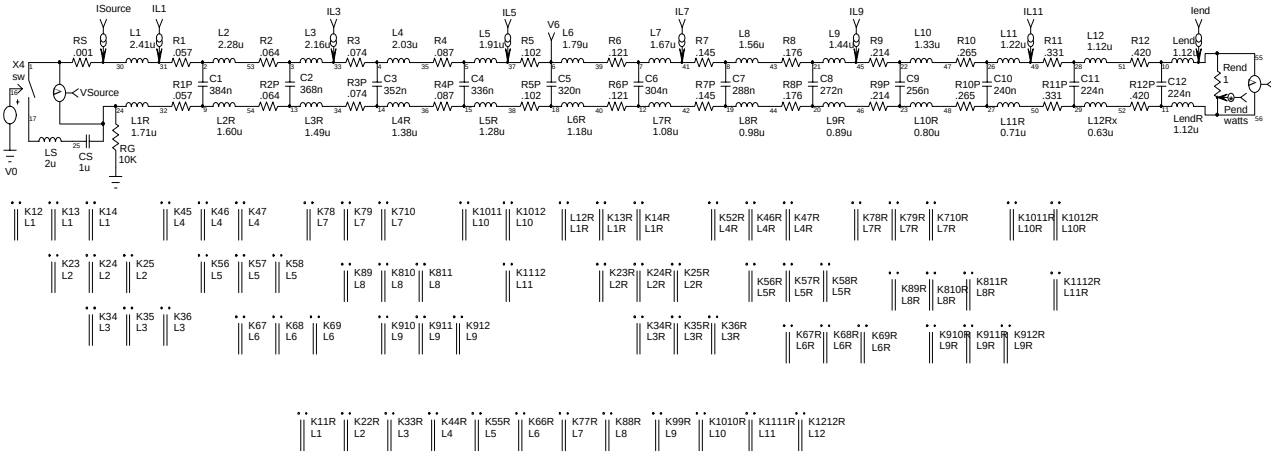

Figure 14. SPICE circuit diagram used for modeling PMWAC

The performance of the accelerator was assessed in several ways. The key parameter, of course, was the magnetic field produced,` and this "bottom line" was easily evaluated by an on-axis B-dot probe. For comparison to electrical circuit modeling, voltages at various points along the accelerator were also made. It was possible in this way to obtain an accurate model of the accelerator. The parameter input into the initial SPICE calculations (capacitance, inductance, mutual coupling, resistance etc.) was based on experimental measurement on the actual accelerator. To simplify the modeling, each coil turn was treated as a lumped L, C and R. The mutual coupling was calculated between the various turns. It was found that coupling between coils separated by more than 2 coils was negligible. No change from the initial input parameters, or a change in the model circuit parameters were necessary to produce an accurate match to the experimental measurements. The SPICE circuit diagram for the 12 coil PMWAC constructed is shown in Fig. 14. Base-lining the model to the experiment allowed for the model to be used to explore different regimes of operation without constructing a new accelerator.

The discrete nature of the coils does manifest itself in one regard. For a transmission line with a continuous inductance and capacitance, the dispersion is a minimum and only dependent on the resistive dissipation in the line. The upper bound in frequency is set by this dissipation The lower frequency of course is set by proper line termination. For the discrete transmission line, there is dispersion. The dispersion equation for discrete elements is given by:

$$\omega^2 = \frac{2(1-\cos k)}{LC}, \qquad (9)$$

where L and C are now the inductance and capacitance per section. The dimensionless wave number is given by:

$$k = \frac{2\pi h}{\lambda} \tag{9b}$$

where the section spacing is given by h and λ is the wavelength of the wave. This dictates that the rise in the current pulse be longer than the than the cutoff wavelength given by:

$$\lambda = 2h \tag{9c}$$

In the limit of very short coil lengths, the inductance approaches that of a loop, where the inductance depends primarily on the loop radius. Thus there is a minimum value for L that depends primarily on coil radius only. Consequently, the inductance per unit length has a minimum attainable value, which when compounded with the dependence of velocity on L and C, fixes an upper bound on C. It happens that the maximum useful capacitance is twice that is obtainable with known dielectric materials (barium titanate). If more capacitance is added to the line from an external source, one must then consider the effect of the inductance of the connecting leads and circuit. The dispersion relation is modified in the following manner:

$$\omega^2 = \frac{2(1-\cos k)}{\left[L + 2L_{ext}(1-\cos k)\right]C} \tag{10}$$

It can be seen that the connection inductance L_{ext} adds to the dispersive nature of the line as well as slows the wave speed. If the wavelength of the wave is large compared to the coil section length, the dispersive nature of the discrete line is not as important. This is almost always the case for plasma acceleration. A sharp rising pulse has a negative effect on the FRC, in that it excites sonic waves inside the plasmoid, which can cause enhanced particle loss. The energy in the wave is taken out over the entire accelerator so there is little reason to put the energy in quickly (short pulse). The externally placed capacitance is thus an option and would allow for a simple way to vary the wave velocity (Isp) and magnitude (thrust). Capacitance could be switched in or out with simple mechanical contact switches, since the variation in Isp and thrust required for a deep space mission is measured on the timescale of a days, not microseconds.

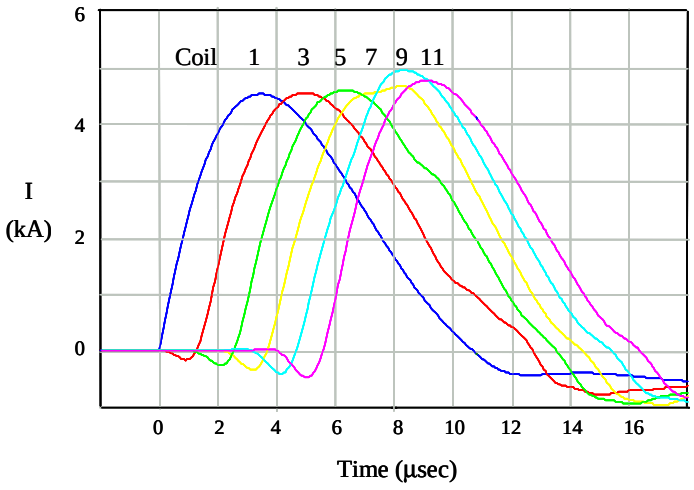

Figure 15. SPICE calculation based on Fig. 14.but without the large coil resistance values (i.e. no plasma).

A sample run of the SPICE simulation is shown in Fig. 15. The pulse shape was determined by the value of the connecting inductance, L_S of the primary storage capacitor, C_S in Fig. 14. As can be seen from the current in the various coils as the wave propagated down the accelerator, λ >> coil spacing. The wavelength was similar to that observed in the PMWAC experiments at high voltage. One might assume that the small negative current that is observed prior to the main current pulse is the result of some dispersion of the high frequency components of the initial wave. In fact, it is due to the mutual coupling between coils. If the coupling

between the coils is eliminated from the calculation, the negative current feature disappears. It was found that the magnitude of this reverse current is a sensitive function of the coil mutual coupling. The observation of this reverse current in the actual accelerator was thus a good check on the calculated coil coupling. The reason for the reversal is that for a coil ahead of the wave has an uncharged capacitance and thus appears as a "shorted turn" or closed loop. With the rise in current in an adjacent coil to the downstream coil, Lenz's law demands that a current in the opposite sense oppose the flux from this current in order to maintain the flux in the downstream coil unchanged. This current does reverse charge the capacitance, so that the resulting field is actually in the opposite direction.

There is an advantage in having this reverse field. The force on the FRC it should be recalled [eq. (2)], is due to the difference in axial magnetic field across the FRC. The effect then from the coil mutual coupling is an enhancement in the field gradient and thus the force on the FRC. The actual downstream field will not be negative since there is a positive quasi-steady bias field that is produced in the accelerator prior to the passage of the FRC. This bias field is a low voltage, very long wavelength field that is easily produced prior to the arrival of the FRC when the accelerator is energized.

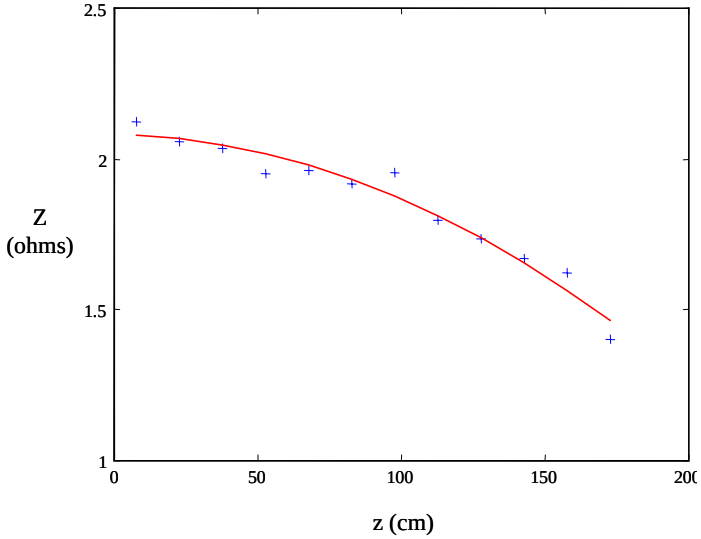

Figure 16. Line impedance measured at each coil along accelerator (+), and calculated impedance from circuit parameters (line),

The coil was operated first at low voltage so that the basic behavior of the wave could be observed with voltage probes attached to various parts of the coils. As with any transmission line, the line must be terminated resistively in its characteristic impedance Z [see eq. (3)]. The reactive impedance, Z_i for each coil was measured as well as calculated from the coil geometry, mutual coupling and capacitance. The results for both are shown in Fig. 16. In order to have the wave velocity increase along the accelerator length, the L-C product must decrease. If the coil segment length is larger than the coil radius, the inductance will decrease with the square of the radius. Assuming a constant capacitor density at the periphery of the coil for all the coils along the accelerator (which indeed was the case), the capacitance will decrease only with the radius. With the length of each coil held constant (constant turn density), the accelerator impedance, $Z \propto r^{-1/2}$. With the coil radius reduced linearly with axial position z, one has $Z_i \propto z^{-1/2}$. In the same way, the variation in wave speed, $v_p \propto z^{3/2}$. In the actual accelerator built, the coil elongation (coil length/radius) ~ 1 at the start of the accelerator, so that the inductance dependence on radius departed from simple r^2 scaling assumed above. The actual wave velocity was found to increase linearly with axial position (constant acceleration).

Of course it was not necessary to reduce the coil radius to accomplish the velocity increase. Increasing the coil length also will decrease the inductance, but unless the capacitor density is decreased, the inductance reduction will be offset by an equal increase in capacitance.

The coil impedance would however still drop allowing the current (and thus magnetic field) to increase.

High voltage testing was conducted with a simple air gap spark switch with the charging capacitor at ~ 14 kV. The on axis magnetic field that was observed with the first coil voltage of 9 kV is shown in Fig. 17. It can be seen that the effect of the axially decreasing coil impedance (the inductance falling faster than the capacitance) caused the field to actually increase as the wave propagated down the accelerator. (The significantly lower field in the first coil is primarily due to the field drop-off at the end of a solenoid.) Even though the current amplitude may rise only slowly along the length as seen in the SPICE calculations of Fig. 15, the actual field depends on the coil geometry. As the coil radius decreases, the coil elongation increases which causes the field on axis to rise even faster. The magnetic field on axis calculated from the currents found from the SPICE calculations is shown in Fig. 18. It can be seen that it produces a result very similar to that obtained experimentally.

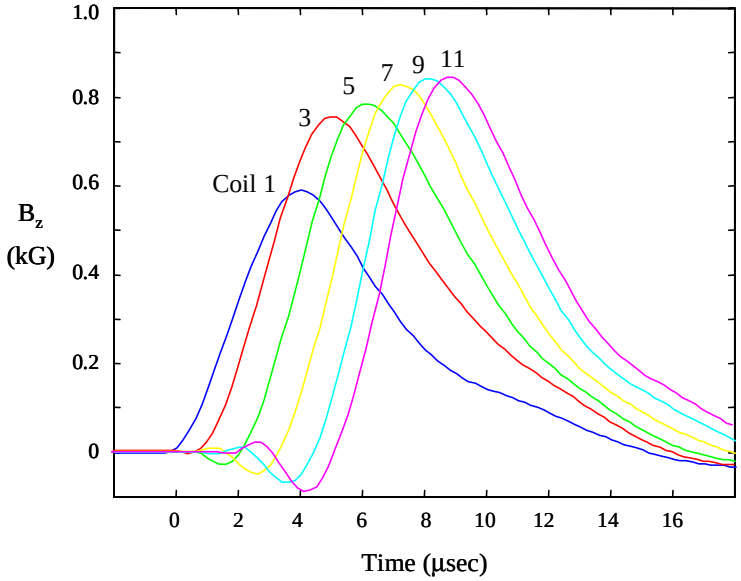

Figure 17. Measured on axis magnetic field under the coil turn indicated. Coils were located every 0.15 m.

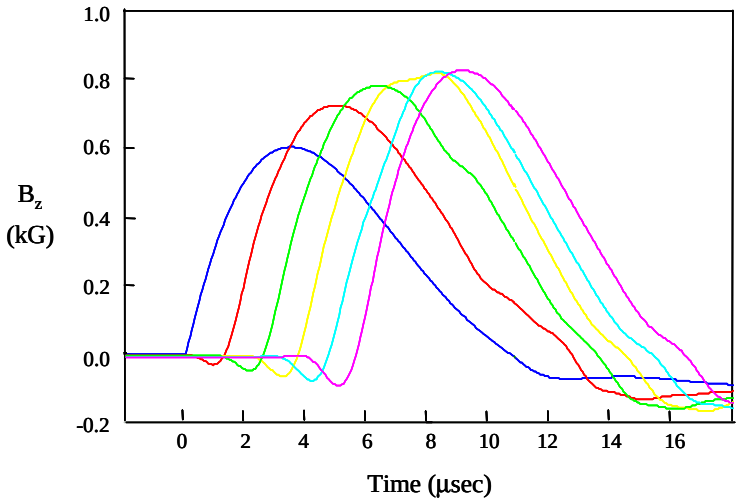

Figure 18. Calculated magnetic field on axis for currents shown in the SPICE simulation shown in Fig. 15.

The time of arrival of the peak magnetic field under each coil is easily determined since it corresponds to the zero-crossing of the B dot probe signal. A plot of the arrival time for the peak field at the center for all of the coil segments is found in Fig. 19. From this data one can calculate both the velocity and acceleration of the magnetic wave. As was stated earlier, the acceleration was found to be nearly constant (quadratic fit) and was identical to that found in the SPICE calculations. Due to the non-linear behavior of the spark gap resistance, the initial voltage waveform that was applied to the accelerator experimentally was somewhat different than that used in the calculations, but the voltages and characteristic behaviors were clearly the same for both. From Fig. 19 it can be seen that the wave speed increases by a factor of 2.3 from the first to last coil. An FRC would then, in traversing the accelerator, gain factor of 5 in energy.

It should be noted that the accelerator had to be tested without a load (i.e. without a plasma). The unloaded line had an extremely high Q (~ ωL/R). due to the low dissipation in both the capacitors and copper coils. At high power (voltage) the accelerator was normally terminated into its characteristic impedance to avoid ringing. Operation at lower voltage was also carried out, and a good measure of the accelerator behavior was obtained by driving the accelerator with a square voltage pulse. This was possible at low voltage with a pulse generator. Although the very low accelerator impedance (~ 1.6 ohms) appeared as a short to the pulser, which was meant to drive 50 ohm loads, the waveform obtained was somewhat like a square wave (see Fig. 20). Driving the input to the first coil of the accelerator in this manner, with the final coil inner turn output tab directly connected to its outer turn input tab (i.e. shorted termination), the magnetic wave was observed to travel back and forth for several hundred microseconds before decaying away (see Fig. 20). The decay of the highest frequency components of the square wave input after several transits is more likely due to resistance in the waveform pulser clip-on connections than dissipation in either the capacitors or inductors. These elements have a high Q well into the many MHz range.

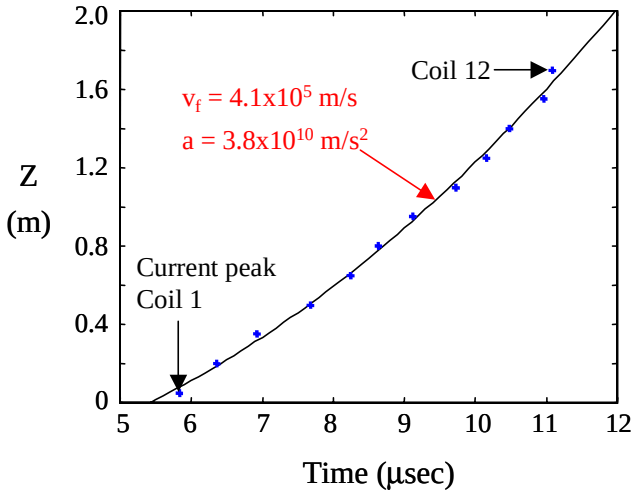

Figure 19. Arrival time of the peak magnetic field under each coil (+). Curve is best quadratic fit to data.

The need for a terminating resistance would be somewhat energy inefficient since all of the energy remaining in the wave after acceleration would be dissipated. When the plasma is added to the accelerator however, the wave will see a significant resistive load during acceleration. During plasma acceleration, at any point along the line, the plasma will act as a load where the energy lost from the circuit at that point will be equal to the kinetic energy gained by the FRC. In this way almost all of the energy is removed prior to the wave arriving at the end of the accelerator. The plasma loading was simulated by adding the appropriate resistance at each coil (see Fig 14). With a

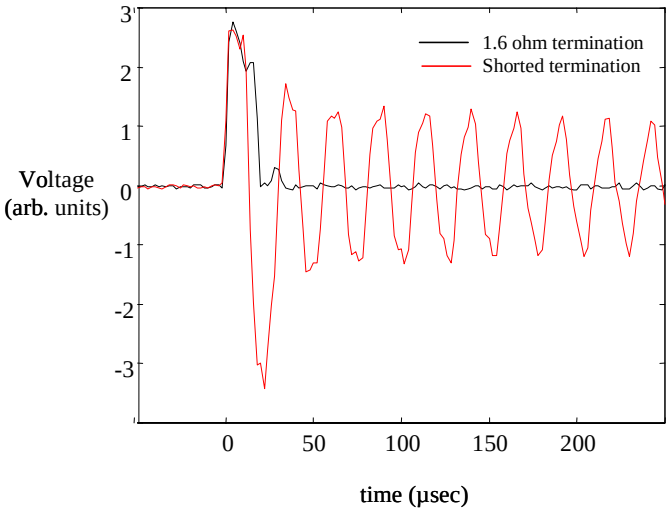

Figure 20. Voltage at the input to the first coil segment of PMWAC for a shorted termination and into the line overall characteristic impedance.

constant plasma acceleration, most of the energy is extracted in the last few coils. The resulting current waveforms, calculated in this manner to include plasma loading, are shown in Fig. 21. For good efficiency, the wave should be strongly damped, but not so much that there isn't sufficient field at the end to provide the needed force to maintain the acceleration [see eq. (2)]. With the line properly loaded, the line can be terminated in a final coil that acts as a low resistance current return only. This type of termination causes any remaining wave energy to be reflected with a subsequent large rise in field near the end of the coil. Because of this, the drop in field at the end of the coil is much reduced from the resistively terminated line. In fact the field actually increases in the last coils as can be seen in Fig. 21.

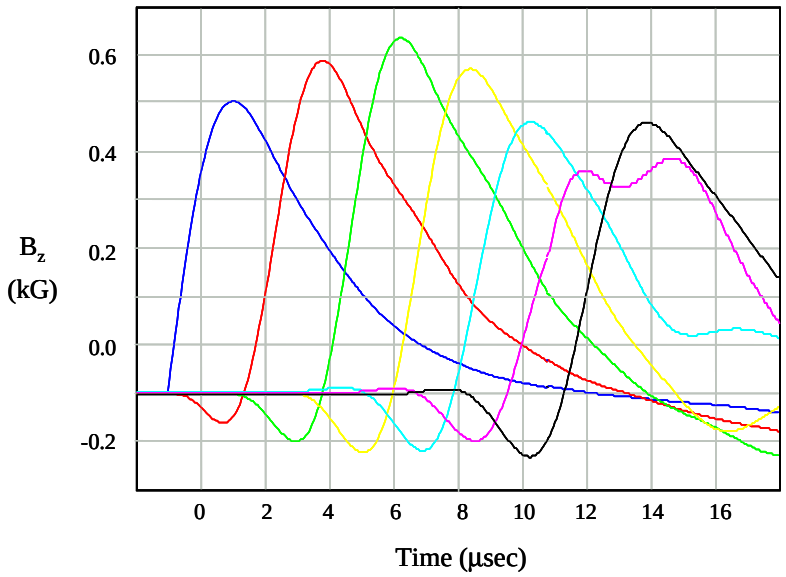

Figure 21. The calculated on axis field with a plasma loading reflecting the increase in FRC kinetic energy at the wave speed. The line is terminated in a low resistance, unlike the unloaded fields of Fig. 15.

The waveforms from the SPICE calculation were used as input waveforms to a 2D resistive MHD calculation to check the validity of the SPICE results. In this way the plasma acceleration could be checked in a more realistic and rigorous manner. The FRC acceleration was as expected. The initial force that the wave could exert on the FRC is much greater than what is necessary so that the FRC stays well in front of the wave. It is only near the end where the wave delivers significant energy to the FRC that the wave amplitude at the end of the FRC rise.

The MHD calculations were employed to study the dynamics of the wave acceleration process. For instance, the initial input acceleration parameters could be varied by changing the FRC mass or flux. For flux greater than what that was necessary [from eq. (2)], the FRC would achieve a much higher velocity initially and move out ahead of the wave. Since no wave force was applied under these circumstances, the FRC would coast at constant

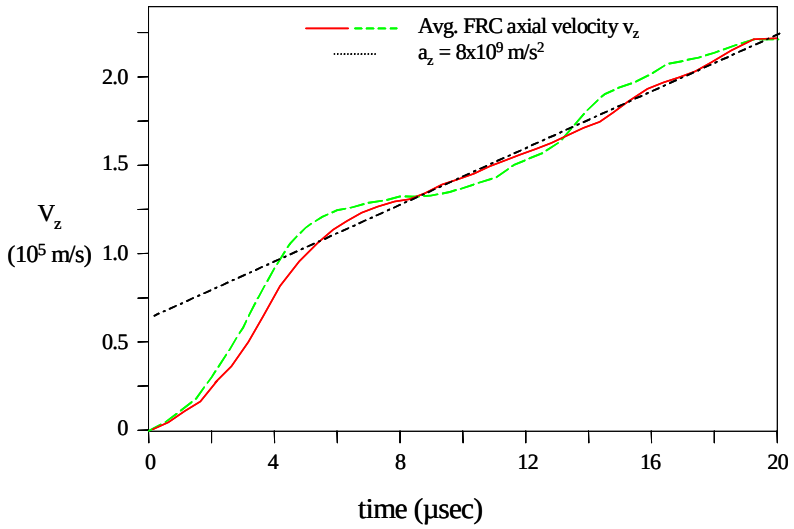

Figure 22. FRC velocity from 2D MHD accelerator calculations. Red trace reflects calculation for FRC with well-matched mass and flux to accelerator fields. Green dashed curve reflects FRC where initial flux was increased by 30%.

velocity. The wave, increasing in velocity, would eventually catch up and impart a somewhat greater than needed force due to the mismatch in speeds. A small oscillation about a constant acceleration was observed (see Fig. 22). The calculations in Fig. 22 were performed for an accelerator with twice the turn density as the prototype (n= 6 m^{-1}). This reflects the intermediate n between that constructed and that appropriate for the relatively low Isp mode discussed in Table I. This self-correcting feature should make the proper acceleration much easier to achieve since the initial plasma conditions need not be so critical. The resulting acceleration of the FRC from the full 2D MHD calculations based on the SPICE electrical calculations is shown in Fig. 23.

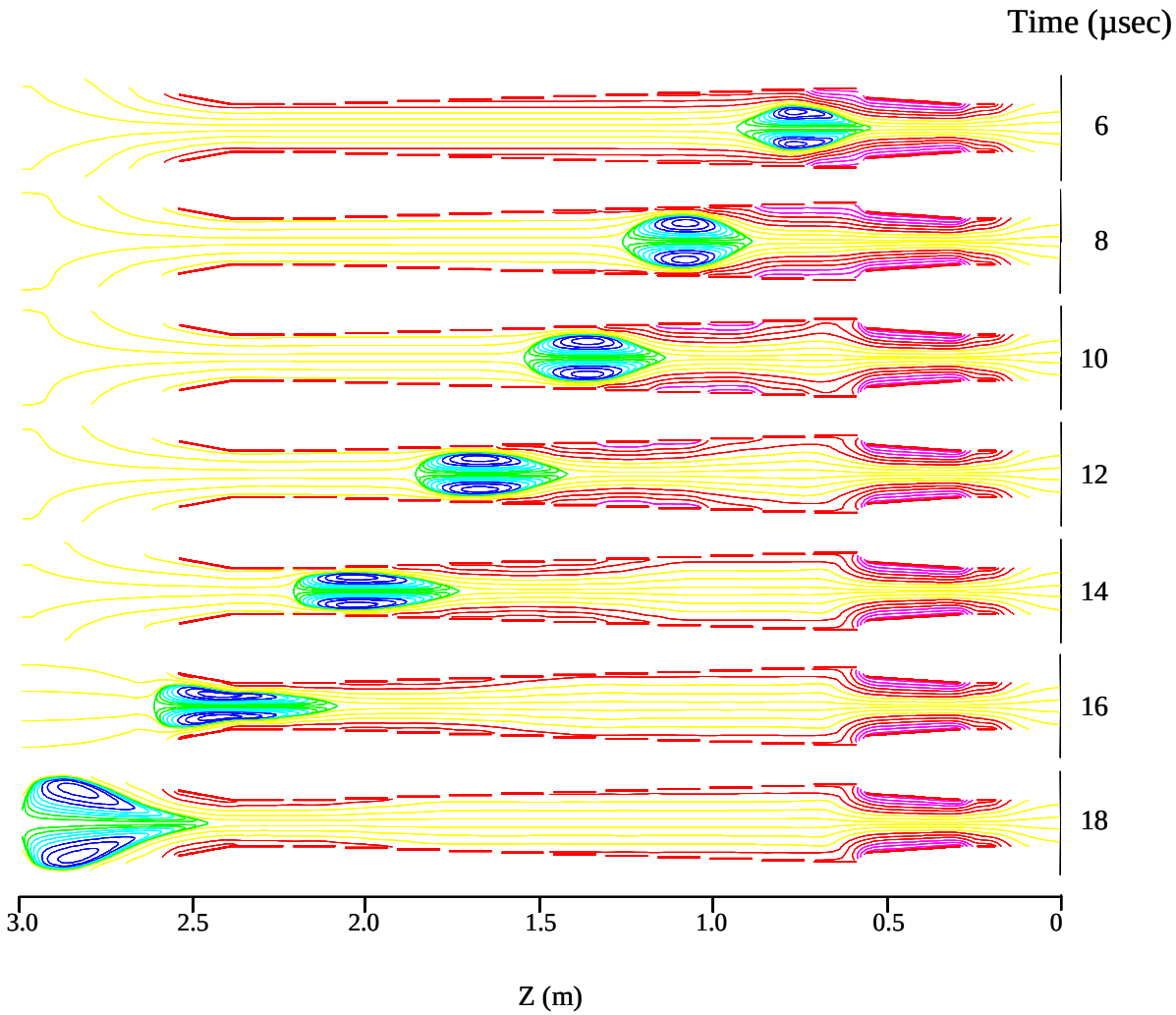

Figure 23. Plot of flux contours at various times during the acceleration of an FRC in PMWAC. Accelerator coil voltages were specified by output from SPICE circuit analysis.

Fusion Rocket using PMWAC

There is another very important role for PMWAC in addition to that of a high power, high Isp, high efficiency electromagnetic thruster. That role is the key enabling technology by which magnetic fusion energy can be made directly available for deep space missions. The manner in which fusion can be accomplished in the near term, at low capital cost, and in a manner ideally suited for space propulsion will now be outlined.

The critical issue for space-based fusion is not so much one of scientific feasibility as viability. The specific problem is that all fusion technologies currently being pursued involve extremely massive facilities, and reach fusion conditions for plasma energies in the gigajoule range. Satisfying the requisite energy confinement requirement to yield a gain in energy from fusion (e.g. the Lawson criterion) the power produced is in the multi-gigawatt range. While this large a power source may sometime in the distant future be required for interstellar missions, the nearest term manned mission, say a rapid mission to Mars would require far less an investment. To make fusion energy in space a viable possibility, a small mass, lower power fusion system must be developed. The conventional regime of Magnetic Fusion Energy (MFE), with plasma density n ~ 10^{20} m^{-3} and magnetic field provided by superconducting magnets, has been

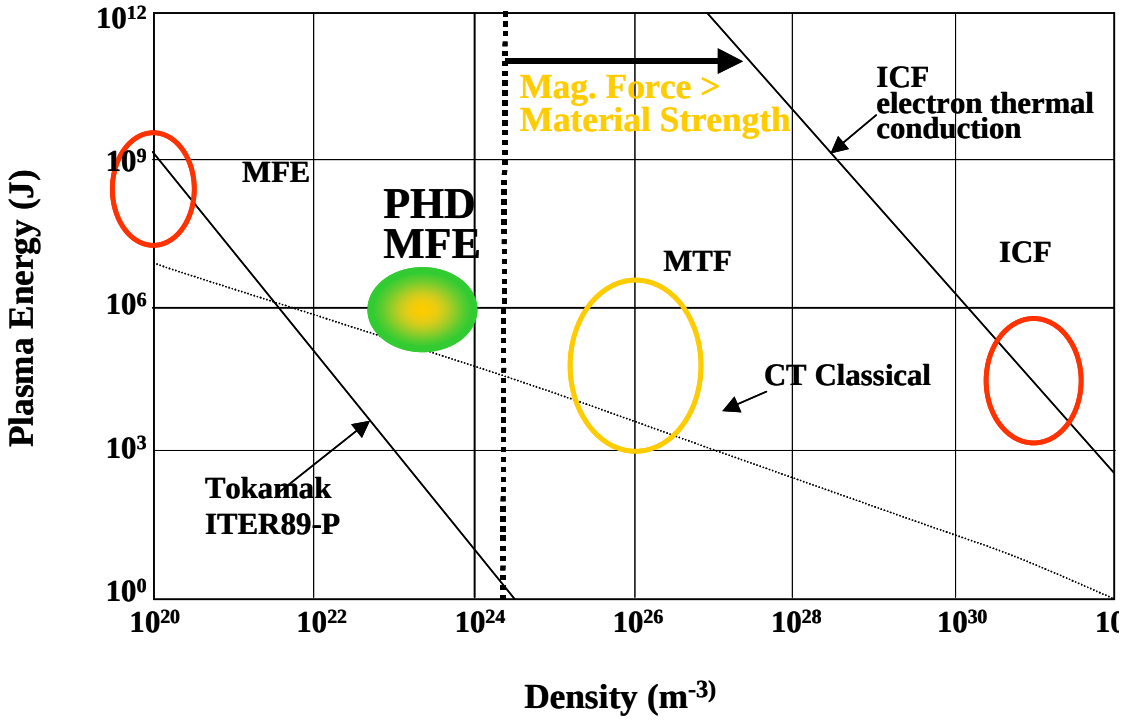

Figure 24. Energy requirements vs. fuel density for various configurations and transport assumptions assuming $n\tau_E$ = 3x10^{14} cm^{-3} sec, T = 10 keV, and poloidal β = 1.

relatively well explored. Tokamaks are the major devices studied in MFE, and tokamak research has tremendously advanced our understanding of plasma physics. The International Tokamak Experimental Reactor (ITER) design illustrates the technology and cost for an ignited plasma demonstration in the MFE regime. The estimated $10-billion price for ITER calls into question whether fusion can ever be developed based on tokamak-like technology. Another approach to fusion, Inertial Confinement Fusion (ICF), represents a good alternative to MFE in that the

regime of density and pressure is completely different, the physics issues are quite distinct, and the technology required has fairly little in common with a tokamak-like system. Thus, the issues those are likely to emerge as limitations for one approach are unlikely to apply to the other. The cost of developing ICF is also high. The price of the National Ignition Facility (NIF), which will demonstrate ICF ignition, is over $2 billion, and the system size is also extremely massive.

There is another regime, which is between MFE and ICF, and where there has been a recent surge of interest. This is the density regime intermediate between MFE and ICF. The region is shown graphically in Fig. 24. The excitement in higher density regimes for magnetic fusion has been spurred by the plan undertaken by the Los Alamos National Laboratory (LANL) and collaborators to perform a proof of principle experiment at very high density (10^{26} m^{-3}). The fusion system that they have proposed is referred to as Magnetic Target Fusion (MTF). Here, the high-density fusion plasma is produced by imploding a metallic liner on an FRC target, which would be formed and translated into the liner prior to implosion (yet another application for the FRC!). There are many difficulties with this particular approach for spaced based fusion. First there is the huge system mass associated with a necessarily high voltage, high energy, pulsed device. Also, the desired density and temperature range for the final plasma requires a confining magnetic field pressure that is well in excess of the yield strength of any material. The device essentially blows itself up. And finally, even if useful energy could be produced from MTF, the rep rate for such a system seems doomed to << 1 Hz.

There is however a high-density regime that is accessible, and can be reached by a natural extension of PMWAC, avoiding all these problems. This regime hereafter referred to as the Pulsed High Density (PHD) regime of MFE. The upper boundary of this regime remains below the density limit imposed coil material strength limitations. In examining past published data, it was realized that, given no better than the confinement scaling observed for FRCs to date, it was not necessary to raise the density any higher than 10^{24} m^{-3}, where the FRC energy is only a few hundred kJ, and achieve significant fusion gain. At this energy level, pulsed operation at high rep rate is quite feasible.

The gain G for a pulsed reactor is proportional to the time that the plasma density and temperature remain in the range for fusion burn. With $n\tau_{burn} \sim 1x10^{20}$ m^{-3} sec, the gain relative to plasma energy of the DT pair plus electrons is around 3, enough to allow for net gain with reasonable conversion efficiencies. A higher gain would desirable for a terrestrial fusion reactor ($n\tau_{burn} \sim 3x10^{20}$ m^{-3} sec), but in space, significant power beyond what can usefully be converted to thrust power is not needed, and would just create more of a waste heat problem.

The total power loss per unit volume during burn is conventionally written as $3nT/\tau_E$, where τ_E is the global energy confinement time. To obtain the minimum possible system size one desires $\tau_E \sim \tau_{burn.}$ That is, if τ_E were much less than τ_{burn} the fuel would cool before it burned. On the other hand if τ_E were much larger than τ_{burn}, the plasma should be made smaller to equalize the two, which requires less energy. Thus one has $n\tau_E \sim n\tau_{burn} \sim 1x10^{20}$ m^{-3} sec. This criterion can be used to determine the plasma confinement time at the target plasma density of $5x10^{23}$ m^{-3}, which implies. $\tau_E = 2x10^{-4}$ s.

With the above criteria for burn, the minimum FRC size and energy can be determined from the confinement scaling for FRCs. Considerable data has been accumulated from various FRC experiments that span over two orders of magnitude in density and an order of magnitude in radius. The observed particle confinement from all experiments yields the following scaling[7]:

$$\tau_N = 2.2x10^{-15}\, x_s^{0.8}\, r^{1.6}\, n^{0.6} l_s^{0.5}, \quad (11)$$

where l_s is the FRC length and x_s is the ratio of FRC radius, r, to coil radius, r_c. The FRC density ($5x10^{23}$ m^{-3}) and temperatures ($kT = (kT_e + kT_i) = 20$ keV) are given by the requirements for burn and material yield considerations. Assuming a reasonable coil filling factor, $x_s = 0.8$, which has been readily attained in experiments at the University of Washington[10], and the scaling given in eq. (11), the FRC radius is determined with the result

$$r = 1.2 \text{ cm}. \quad (12)$$

For an FRC elongation of $l_s \sim 30r$, the FRC volume, particle inventory and energy can be calculated:

$$N = 30\pi \langle\beta\rangle n r^3 = 5.5x10^{19}, \text{ where } \langle\beta\rangle = (1 - 0.5x_s^2) \quad (13)$$

$$E_p = 3/2\, N\, kT = 260 \text{ kJ}. \quad (14)$$

With the fusion gain, G. and a pulse rep rate f_p, the thrust power represented by the conversion of FRC plus fusion energy into directed flow is

$$P_t = \eta_p\, f_p\, G\, E_p, \quad (15)$$

where η_p represents the conversion efficiency of the fusion energy. To increase the fusion gain, (or equivalently burn time), only a small increase in plasma radius is required due to the strong $r^{2.4}$ confinement scaling [see eq. (11)]. The conversion efficiency of the fusion neutrons is likely to be no better than 40%, but virtually all the fusion alpha energy is converted to thrust since it is magnetized inside the FRC. The final efficiency would thus be ~ 55 %. For a fusion gain of 20, the FRC radius is increased to 2.7 cm and the FRC energy to 1.3 MJ. With a low rep rate of only 10 Hz, one has from eq. (15) a thrust power of 140 MW.

It should be noted that the particle inventory given in eq. (13) is in the range of those readily obtained in past FRC experiments, and the energy only a factor of a few larger.. The significant difference of course is that the plasma energy and inventory have been obtained at an order of magnitude larger radius in past experiments. The question is how to get here from there, and that is where PMWAC plays a key role.

The method by which the plasma density and temperature can be brought to the fusion conditions described above is to start with a much simpler and much lower energy FRC plasma source that can be repetitively pulsed. The energy necessary for burn is transferred to the FRC in the form of translational energy, which is developed in the accelerator (PMWAC). The simplicity of this approach to fusion lies in the fact that the directed energy of the FRC mass, E_d is much greater than the FRC internal energy, E_i. Since E_d is in the form of a coherent translational motion, the confining magnetic fields, as well as accelerating fields, need to be no greater than required to contain the low-pressure FRC generated in the source coil (~ 0.4 T). This leads to a tremendous reduction in magnet mass as well as stored energy requirements for the accelerator. The conversion of the FRC directed energy into thermal energy occurs only after the FRC has reached the burn chamber where the FRC is slowed and compressed to fusion conditions. This chamber, which has a high magnetic field can be steady state and could thus generated by a superconducting magnet. A schematic of the basic process is shown in Fig. 25.

The maximum vacuum fields for all the coils is less 0.4 T that can be produced in the

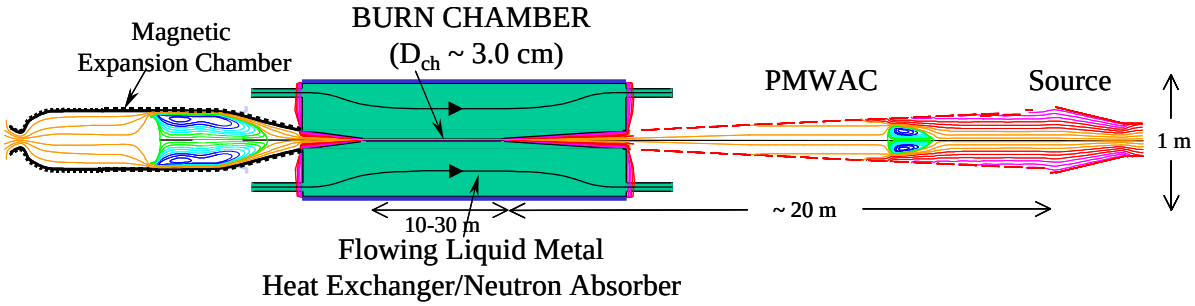

Figure 25. FRC based fusion rocket.

PMWAC, and the voltages employed during the acceleration are within the range of either stacked solid state IGBT switches[11], like those used in the PMWAC prototype, or ignitron switched given the low rep rate. The FRC is not completely decelerated into the burn chamber. The advantage of leaving a residual velocity is that during burn, the fusion neutrons and plasma radiation can be spread out over a much larger volume. Converting ~ 90 % of the plasma translational energy into thermal leaves enough residual velocity ($3x10^5$ m/s) that the FRC during the ~ 100 μsec burn can sweep out several meters, thus increasing the volume of thermal blanket by a factor of 30 or more over a stationary burn. In addition, the long burn tube allows the neutron-absorbing blanket to shield the entire rocket, and all but a tiny area near the symmetry axis area from fusion neutrons. The FRC emerges from the burn chamber into an expansion chamber that has a weaker magnetic guide field to maintain the magnetic plasma-vacuum insulation. The plasma expansion reconverts the thermal energy of the fusion temperature FRC back into directed axial velocity as well as directly into electricity through the flux compression of the expansion chamber field. The electrical efficiency of the flux transferal into inductive energy storage is much higher than the thermal cycle, and sufficient energy can be extracted at higher fusion gain to significantly reduce the thermal cycle power conditioning that would be required. This would save considerably on rocket mass, as the power conditioning system is the only system with any significant mass in the entire rocket.

The plasma velocity on ejection from the expansion chamber through the magnetic nozzle would be greater than that on entry due to the fusion heating (>10^6 m/s). This is too high an Isp for all but the most ambitious missions, but it can be easily lowered and exchanged for increased thrust by injecting frozen hydrogen 'snow' into the expansion chamber prior to the FRC pulse. With the passage of the FRC, the snow is ablated and ionized inside the FRC in much the same way that large Tokamaks are fueled with frozen deuterium pellets. This new plasma is entrained and magnetically trapped within the magnetic envelope of the FRC, which cools and slows as the momentum is transferred from the original FRC plasma to the new plasma. The FRC is then ejected with a significantly increased mass and at the characteristic velocity for maximum thrust power and efficiency. As the FRC experiences the lower magnetic field outside the nozzle, the FRC is accelerated out of the expansion chamber with the conversion of all of the remaining FRC thermal energy into directed energy. There is no need for magnetic detachment, since the plasma is self-magnetized and isolated from the rocket fields as it is in the PMWAC thruster.

Program for development of PMWAC

The main thrust (no pun intended) of a future research program will be the experimental verification of the PMWAC concept with a demonstration of plasmoid acceleration. In addition to this achievement, there must also be the technical milestone of a thrust and Isp measurement. Finally, there is the important developmental challenge of the operation of the PMWAC at high power for a sufficiently long period of time in a space-like environment to evaluate both the thermal behavior and reliability of the device for the deep space missions that it is envisioned for. These three goals then form the basis for the research to be performed under phase II. The first two objectives are closely linked and, as will seen, can be accomplished in the same experimental setup. The first task would be accomplished during the first year. The thrust measurement would follow in the first half of the second year, and the final task would be completed by the end of the second year. This task would be initiated in the experimental configuration where the long-pulse operation of the device could be debugged and tested. The final testing would require a much larger facility that could handle the megawatt plasma throughput in a space-like setting. Sufficiently large vacuum tanks exist at several NASA sites, and a suitable arrangement with NASA for further testing would be sought. These three these objectives will now be described in greater detail in the order in which they will be accomplished.

Experimental Apparatus

In order to perform the plasma test, a vacuum chamber must be constructed. Since the most important task initially is to observe and optimize the accelerator for plasma acceleration, it makes far greater sense to build a vacuum chamber inside the accelerator than the opposite. The final space-like test of the accelerator will be done only after the PMWAC design has been verified and optimized. The vacuum chamber must also accommodate the source. The source coil that has already developed was made to be compatible with an external mounting. The source coil however no longer exists in a usable state. Although a similar source coil could be reconstructed, there is a very promising FRC formation technique that has recently been developed by the author at the University of Washington[12]. It is the intent of the investigators to develop this new source with the previous source as a clearly viable backup. There are several advantages to this new source, and this different approach will now be briefly described.

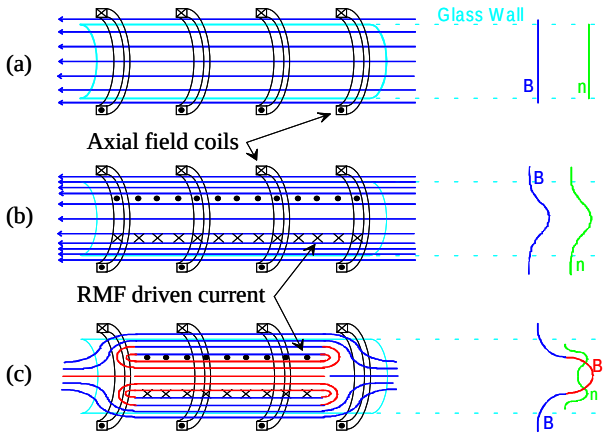

Figure 26. RMF formation sequence (a) Begin with a constant axial magnetic bias field. (b) A RMF field is applied driving an azimuthal current in the direction opposite to that in the axial field coils. The plasma is both ionized and ohmically heated by the current. (c) Field reversal is achieved when a sufficient electron density is achieved.

The method of formation differs from that in Fig. 5, in that no fast reversal of the axial magnetic field is required. Instead, the field-reversing currents are generated inductively by a Rotating Magnetic Field (RMF) in the manner described in Fig. 26. This method does away with both the plasma wall contact and flux loss associated with reversal. Without these two drawbacks, the RMF FRC startup approaches the ideal loss-less formation desired, with the only loss being the unavoidable one from ionization. The RMF is produced by two oscillating Helmholtz coil pairs set at right angles and positioned external to the source coil with a phase shift of 90 degrees (see Fig. 27). The literature on the physics base for RMF current drive is extensive[13], but a starting point for understanding the current drive process is the generalized Ohm's Law, where it will be assumed for the moment that the ions form a fixed uniform background and the **u×B** term can be ignored:

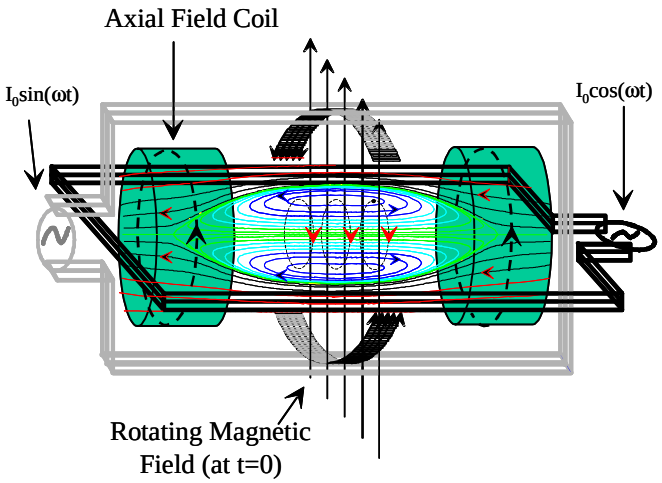

Figure 27. Illustration of RMF drive concept for FRC generation

$$\mathbf{E} + (\mathbf{u}\times\mathbf{B}) = \eta\mathbf{j} + \mathbf{j}\times\mathbf{B}/ne = \eta[\mathbf{j} + (\omega_{ce}/\nu_{ei})\mathbf{j}\times\mathbf{e_B}] \qquad (16)$$

where B has oscillating components in the θ and r directions due to the RMF at a frequency ω_{RMF}, and a steady axial field provided by the axial field coils (see Fig. 27). If the Hall term $\mathbf{j}\times\mathbf{B}/ne$ is small compared to the resistive term, $E_\theta = \eta j_\theta$ is positive, and from Faraday's law, $d\phi/dt$ is negative and the FRC decays. With the Hall term dominant, E_θ, for sufficiently small η or large $\langle j_z B_r\rangle$, can be negative with a subsequent increase in flux.

The solution of Ohm's law, neglecting the Hall term, is characterized by the RMF penetrating a distance $\delta = (2\eta/\omega\mu_o)^{1/2}$, which is the resistive skin depth for a conductor in an RF field. However, the regime of interest here is a plasma where $\nu_{ei} << \omega_{ce}$. In this limit, from Ohm's law, $j_\theta \approx -ne\omega$ and $j_z \approx E_z/(\eta\omega_{ce}^2/2\nu_{ei}^2)$. The electrons are in synchronous rotation with the RMF and their response to the axial electric field is severely restricted (small j_z), and unable to screen out the RMF field. From another viewpoint, the co-rotating electrons experience a nearly steady transverse field, and the effective field penetration can be many times the resistive skin depth. The Hall term has a pondermotive component, the $\langle j_z B_r\rangle$ term, acting in the θ direction. Since j_z, B_r, and B_θ vary in time at the frequency ω_{RMF}, the pondermotive force in the θ direction has a steady part and an oscillatory part at a frequency of $2\omega_{RMF}$. From the steady $\langle j_z B_r\rangle$ force, the electron fluid attains a steady value of azimuthal velocity, $v_{e\theta}$ that corresponds to the balancing of the steady accelerating torque by the retarding torque (due to the collisions of the electrons with the ions). In this way a steady azimuthal current density,

$$j_\theta = -ne\omega_{RMF}\, r \qquad (17)$$

is produced.

In the experiments conducted at the UW, the RMF field was observed to penetrate only to

the field null, so the pondermotive force acted only at the outer edge of the FRC. The effect of large internal plasma screening currents (j_z) allowed for the radially acting $\langle j_z B_\theta \rangle$ force to produce a radially inward pressure at the plasma edge. In equilibrium ($E_\theta \sim 0$), the larger $\langle j_z B_r \rangle$ term must now be balanced by $u_r B_z$ and the flow term in eq. (16) cannot be ignored. To achieve equilibrium inside the FRC, where there is no RMF, the axial field pressure must be balanced by a radial inward plasma flow as well. The induced flow opposes the radially outward flow from plasma diffusion and dramatically inhibited particle loss at the separatrix. In the experiments, the particle confinement time increased from ~ 50 μsec to over 1 msec[11]. With the total time from FRC formation to ejection approaching 20 μsec for the high thrust, lower Isp operation mode of Table I, particle loss can lead to a lower total efficiency. Although this plasma loss occurs before it has gained significant translational energy in the accelerator, it can be important since the lost plasma represents the only significant thermal load to the thruster. The use of the RMF formation method assures that there is no plasma flow to the thruster walls at any time during formation.

The PMWAC accelerator would also be rebuilt to take advantage of custom built, higher density ferro-electric capacitors. The coils will also be designed for multi-mode switching as well. The accelerator turns density [n in eq. (5)] determines the wave speed and thus Isp. It is desirable to allow for the accelerator to be operated with different turn densities with a variation of at least a factor of four. With the high Isp condition being the one that was explored in phase I, the turn density will thus be increased by four with switching to allow for operation at the lower turn densities. This should allow for the easier manufacture of the coils as well. The coils will be potted so that they can be operated at higher voltage and in vacuum. The overall length, initial radius, and taper will remain unchanged, as it appears to be about right for a significant rise in Isp and efficiency.

Thrust Measurement

Given the bulk of the PMWAC, and the fact that it will not be mounted inside a vacuum vessel, requires that a different type of thrust measurement than the usual thrust stand measurement be made. Besides avoiding magnetic detachment problems, the ejection of the FRC as an entire entity, allows for an accurate thrust measurement that is more akin to that performed on ballistic objects such as bullets. To this end, the capture of the FRC after ejection in a suspended 'dump' chamber will allow for the direct measure of the thrust provided by the FRC. A schematic of the measurement setup is shown in Fig. 28. In order to have the interaction of the FRC and the dump chamber be inelastic (no plasma escaping after passage into the chamber, the inside of the chamber will be sprayed with titanium from a titanium getter pump. The getter pump is used frequently in plasma fusion experiments for just this purpose. The great affinity of the Titanium for hydrogen allows for all surfaces inside the chamber to act as a pump with no plasma emerging from the surface after contact. The chamber will then act as a ballistic pendulum with the chamber set in motion by the inelastic absorption of the ejected FRC. The motion of the chamber from a single pulse of course will be quite small, but can readily be observed by an end-on visible Michelson interferometer (see Fig. 28). From Table I, one anticipates that the FRC will be ejected with a mass of 10 μg and a velocity of 1.4×10^5 m/s. With a dump chamber mass of ~ 1kg, the increment in velocity after the adsorption of one FRC would be 1.4×10^{-3} m/s (or 1.4 nm/μs) from momentum conservation. For a 600 nm laser, fringe shifts of 0.01 (6 nm) are

measurable without too much effort. Even if the time between FRC pulses were as small as 100μs (a rep rate of 10 kHz), the fringe shift acquired on each pulse would be ~ 0.25. The thrust imparted with each pulse should be easily resolved.

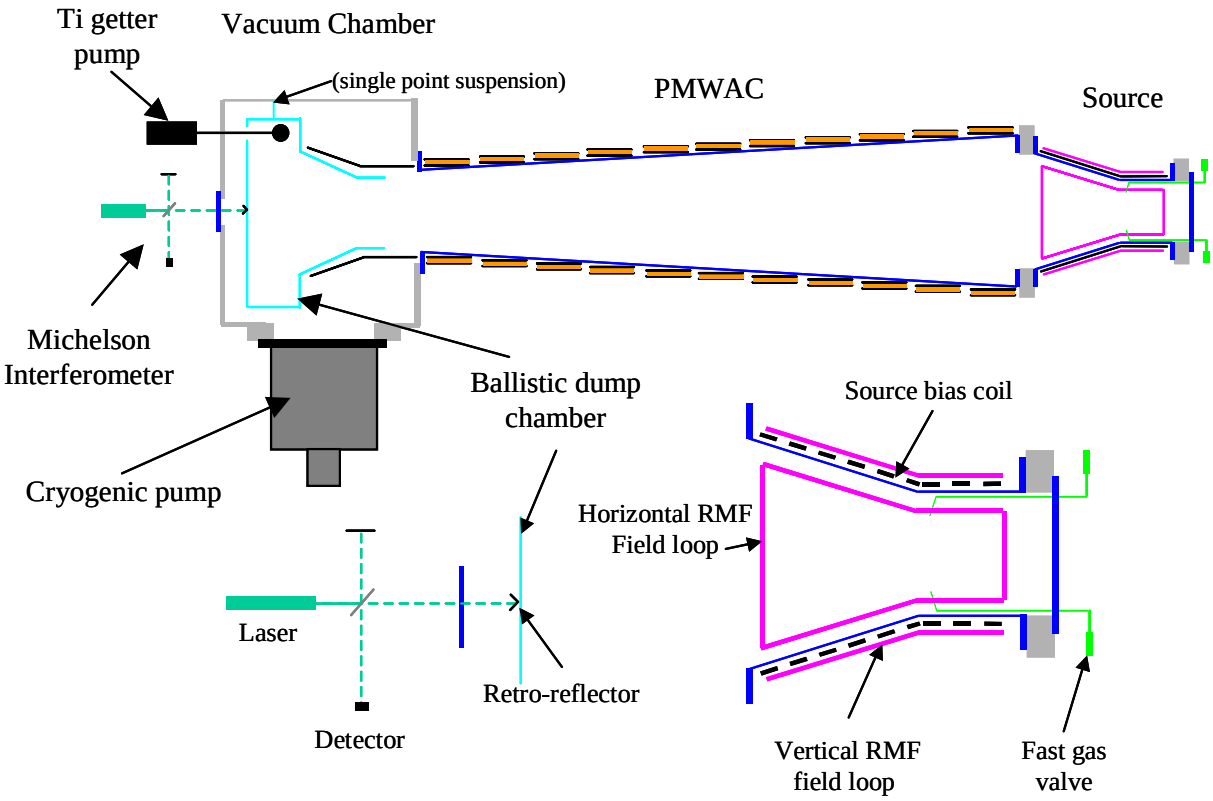

Figure 28. Experimental layout for further tests of the PMWAC thruster

Long pulse train testing

In order to gain some understanding of the thermal behavior and repeatability of a megawatt PMWAC thruster, a sufficiently long period of operation of the accelerator and source must be conducted. Ultimately one would like to operate the device for hours and eventually days. This would require fairly sophisticated power control and conditioning systems, as well as a very significant power bus and cooling system. It is thus beyond the funding level provided for under Phase II. The basic behavior of the thruster regarding reliability and consistency can be learned, however, by operating at full power with a pulse train on the order of several hundred pulses. This should be sufficient to establish the feasibility of steady pulsed operation and indicate clearly how much thrust power is being produced, and where the power is being dissipated within the thruster. Pulse to pulse repeatability can easily be assessed in this way. Information about reliability will come from repeated long pulse operation.

Operation at the 1 MW power would require a pulse train of FRCs moving with 100 J of directed energy, produced at a rate of 10^4 s^{-1}. The total energy that would pass through the system during pulse train of 200 pulses would be on the order of 20kJ, and the pulse burst time would be 20 msec. During this time of operation, it will not be possible to recharge the storage capacitors. In order that the power variation over the pulse burst time is not large, the initial stored energy must be large compared to the energy discharged, so that the initial stored energy must be roughly 100 kJ. For this amount of stored energy, it is reasonable to use high-voltage (20 kV), high energy density (25 kJ) capacitors. In this way only four capacitors will be required.

The time for thermal equilibration within a material varies with the material dimension divided by the sound speed, v_s in that material. For most materials $v_s \geq 1$ m/msec, so that the 20 msec operation time is more than enough time for the thruster to reflect the long term heating rates for the various components. Of course this time is not long enough to reflect the final steady-state conditions. Given that the PMWAC thruster will not be equipped with any thermal control system (radiators, reflectors, cooling, etc.), the final stead-state conditions would not reflect the true thruster performance in any case. The measurement of the power flow however would provide the input required for the design of an appropriate thermal system.

The appropriate diagnostics (voltage probes, thermocouples, etc.) would be added after optimization of the accelerator. With successful operation with long pulse trains, the PMWAC thruster would be ready for full development and testing. This would require a large vacuum chamber with the appropriate power bus and thermal systems. At this level, the research and development would no doubt be at a NASA center where such facilities and expertise is readily available.

References

[1] Robert Sackheim, Melissa Van Dyke, Mike Houts, David Poston, Ron Lipinski, Jay Polk, Robert Frisbee, "*In-Space Nuclear Power as an Enabling Technology for Deep Space Exploration*", 36th AIAA Joint Propulsion Conference, Huntsville, AL, Paper AIAA 2000-3881.

[2] N.R. Schulze, "*Fusion Energy for Space Missions in the 21st Century*", NASA Technical Memorandum 4297, Executive Summary, pg 39 (1991).

[3]. M. Tuszewski, "*Field Reversed Configurations*", Nuclear Fusion **28** (1988) 2033.

[4] L. Johnson and S. Leifer, "*Propulsion Options for Interstellar Exploration*", 36th AIAA Joint Propulsion Conference, Huntsville, AL, Paper AIAA 2000-3334.

[5] F. Chang-Diaz, et al., "*Rapid Mars Transits with Exhaust Modulated Plasma Propulsion*", NASA Technical Paper 3539, (1995).

[6]. J.T. Slough and A.L. Hoffman, *"Acceleration of a Field Reversed Configuration for Central Fueling of ITER"*, Sixteenth IAEA Fusion Energy Conference, Montreal, Canada, 7-11 October 1996.

[7]. A.L. Hoffman, J.T. Slough, "*FRC Lifetime Scaling Based on Measurements from the Large s Experiment (LSX)*", Nuclear Fusion **33**, 23 (1993).

[8] J.T. Slough et al., "*Confinement and Stability of Plasmas in a Field Reversed Configuration*", Phys. Rev. Lettr. **69**, 2212 (1992).

[9] J.T. Slough and R.D. Milroy, "*Diagnostic system for determining the internal structure of a field reversed configuration"*, Rev. Sci. Instrum. **61** 3280 (1990).

[10] J.T. Slough, K.E. Miller, *"FRC Formation and Sustainment using RMF Fields"*, Phys. of Plasmas, **7**, 1945 (2000).

[11] P.M. Bellan *"Spontaneous, Three Dimensional Constant Energy Implosion of Magnetic Mirror Fields"*, Phys. Rev. Lett. **43**, 858, (1979).

[12] K. Okamura et al., "*Development of a semiconductor switch for high power copper vapor lasers"*, IEEE 11th Pulsed Power Conference, pg. 975 (1997).

[13] J.T. Slough, K.E. Miller, *"Enhanced confinement and stability of a Field Reversed Configuration with Rotating Magnetic Field Current Drive"*, Phys. Rev. Lett. **85**, 1444 (2000).

[13] I. R. Jones, "*A review of rotating magnetic current drive …"*, Phys. of Plasmas, **6**, 1950 (1999).